




## Research Article

# Solvothermal synthesis of nanoscale disc-like gadolinium doped magnesium zirconate for highly efficient photocatalytic degradation of rhodamine B in water

S. Akshatha<sup>1</sup> · S. Sreenivasa<sup>1</sup>  · L. Parashuram<sup>1,2</sup> · V. Udaya Kumar<sup>3</sup> · Tadimety Madhu Chakrapani Rao<sup>4</sup> · Sandeep Kumar<sup>5,6</sup> · M. S. Raghu<sup>2</sup>

Received: 24 January 2020 / Accepted: 2 April 2020 / Published online: 10 April 2020  
© Springer Nature Switzerland AG 2020

## Abstract

Highly ordered nanoscale disc-like cubic gadolinium doped magnesium zirconate ( $\text{Gd:MgZrO}_3$ ) was synthesized by facile solvothermal route. The reaction time was found to be crucial in determining the final morphology of disc-like  $\text{Gd:MgZrO}_3$ . After studying the particles from time-dependent experiments, it is observed that, the formation of disc-like particles involved a complex process, in which rod-like or agglomerate particles were favorably formed after the initial thermal treatment. Owing to the chemical instability, they would turn into disc-like particles. After calcination, the generated product possessed good photocatalytic performance for the degradation of Rhodamine B ( $50 \text{ mg l}^{-1}$ ) under UV light irradiation in contrast to morphologies of  $\text{Gd:MgZrO}_3$  and other related state-of-the-art photocatalysts (e.g.,  $\text{TiO}_2$ ,  $\text{ZnO}$ ,  $\text{WO}_3$ ,  $\text{BiVO}_4$ ,  $\text{Fe}_2\text{O}_3$ , and  $g\text{-C}_3\text{N}_4$ ). The catalyst could be used for five cycles, maintaining its efficiency above 94.2%. These capacities made the disc-like  $\text{Gd:MgZrO}_3$  a potential candidate for polluted water treatment. Also, the underlying photocatalysis mechanism of  $\text{Gd:MgZrO}_3$  was proposed through radical trapping experiments.

**Keywords** Gadolinium doped zirconia · Photocatalysis · Rhodamine B degradation · Nanoscale disc

## 1 Introduction

Industrial dye effluents are one of the major sources of water contamination and indicate increasing threat to the environment [1]. Textile and dyestuff industries are continuously releasing the toxic, chemically stable, complex and non-biodegradable dye contaminants into the water bodies. Hence, removal of organic pollutants in water requires devising versatile strategies [2]. Researchers have demonstrated various strategies like adsorption of dye effluents on activated carbon, coagulation, membrane purification and reverse osmosis for

the removal of dye effluents from water. However, all these methods are tedious and produce secondary contaminants, which has to be further treated to avoid pollution. Hence, photocatalytic treatment of dye effluents is one of the most effective approach for the removal of organic contaminants in water [3–6]. In this path, metal oxide nanomaterials showed excellent photocatalytic activity for the removal of organic dyes due to their high physical, chemical properties, high surface area, high surface energy and quantum confinement effects compared to the counter bulk materials. In the past decade, many catalysis researchers attempted to develop

✉ S. Sreenivasa, [drsreenivasa@yahoo.co.in](mailto:drsreenivasa@yahoo.co.in); ✉ L. Parashuram | <sup>1</sup>Department of Studies and Research in Organic Chemistry, Tumkur University, Tumkur 572101, India. <sup>2</sup>Department of Chemistry, New Horizon College of Engineering Affiliated To VTU, Bangalore 560087, India. <sup>3</sup>Department of Chemistry, Siddaganga Institute of Technology Affiliated To VTU, Tumkur 572102, India. <sup>4</sup>Tadimety Aromatics Pvt. Ltd, Hirehally Industrial Area, Tumkur 572168, India. <sup>5</sup>Raman Research Institute, C V Raman Avenue, Bangalore 560080, India. <sup>6</sup>Department of Chemistry, Nitte Meenakshi Institute of Technology, Yelahanka 560064, India.



heterogeneous photocatalysts with bimetallic and trimetallic modifications to improve charge transport properties, electronic structure and porosity for enhanced photocatalytic performance [7–10]. In addition to these properties it is a known fact that, these metal oxides are nature abundant, they show excellent stability under various conditions. However, the major disadvantage of using metal oxide photocatalysts is fast recombination of photogenerated electron–hole system, this leads to ineffective generation of free radicals required for the photo degradation process. This problem can be overcome by creating p–n junction or suitably tuning the band energies of the material. Till date, number of metal oxide photocatalysts have been developed with multi metallic composition and structural features [11–15]. Nanoscale zirconia is an excellent material in the field of catalysis [16], electrochemical sensor [17], photocatalysis [18], solid acid catalyst [19] and fuel cells [20] etc., these properties have imparted for zirconia due to its high surface area, porosity, wide band gap, chemical inertness, thermal stability, abundancy and low cost. These properties of zirconia makes it a material of choice for most of the catalysis researchers. Introducing the metal ions like Mg, Ca, Bi, Sm, Gd with different oxidation state will induce flexibility in the band structure of zirconia. These ions can result in the formation of oxygen vacancy defects thereby altering the electronic, thermal and catalytic properties of zirconia. Also, these dopant ions will effectively control the recombination of photogenerated charge carriers and interfacial charge transfer, as faster recombination is one of the drawbacks of zirconia when it is used in photochemical processes. Out of all these dopant ions Mg draws considerable interest as, magnesium oxide at nano scale posses high defect centers which leads to the formation of  $O_2^-$ , this enhances the photocatalytic performance of zirconia. Further a rare earth dopant gadolinium is localized with half filled f-orbitals act as trap centers for charge carriers and reduce the rate of electron–hole recombination, thus improve the photocatalytic efficiency. There are many methods reported for the synthesis of nanoscale zirconia like co-precipitation [21], sol–gel [22], solid state reaction [23], hydrothermal [24] and solvothermal [25] etc., Out of all the methods solvothermal method is superior in terms of great control over particle morphology and particle size. Keeping in mind all the challenges that are mentioned in the above discussion, herein we report a simple and facile method for the synthesis of a trimetallic gadolinium doped magnesium zirconate ( $Gd:MgZrO_3$ ) via solvothermal process. A detailed characterization of thus prepared material has been carried out, photoluminescence spectroscopy has been used to probe into the defect states of the material. Further  $Gd:MgZrO_3$

has been used for the photocatalytic degradation of Rhodamine B in water. Hence, we propose the novel  $Gd:MgZrO_3$  as a promising candidate in the environmental remediation.

### 1.1 Preparation of $Gd:MgZrO_3$

Disc like  $Gd:MgZrO_3$  (4 mol%) has been prepared by solvothermal method. In the typical procedure, known quantity of the precursor  $Gd_2O_3$  has been digested in conc. nitric acid and the excess nitric acid has been quenched, thus obtained gadolinium nitrate is mixed with  $Mg(NO_3)_2 \cdot 6H_2O$  and  $ZrO(NO_3)_2 \cdot xH_2O$  (46 mol%:50 mol%) in 60 ml of solvent (Water:DMF-1:1 v/v). The resultant solution was ultrasonicated to get homogeneous solution and loaded into a teflon lined stainless steel autoclave and subjected to solvothermal treatment at 180 °C for a given period of time (24–72 h). The supernatant liquid in the final product has been removed carefully by decantation, the product was washed thrice with DMF ( $3 \times 10$  ml) and finally with chloroform. Thus obtained solid was dried at 120 °C, calcinated at 800 °C and stored under vacuum dessication till further use. Following the similar experimental conditions 1, 2, 3 and 5 mol% gadolinium doped magnesium zirconate samples were prepared.

## 2 Results and discussions

FTIR spectra were recorded using Bruker-Alpha spectrometer with spectral grade KBr. Powder X-ray diffraction data was recorded using Rigaku smart lab with Cu-K $\alpha$  as the radiation source. Thermogravimetric analysis has been carried out using PerkinElmer, USA, TGA4000 instrument. BET surface characterization was done using ASAP-Micromeritics porosimeter. Diffuse reflectance spectra (DRS) of the samples were recorded using PerkinElmer UV Winlab Lambda 35 instrument. The morphology and structure of the samples were inspected using Zeiss FESEM instrument. XPS analysis was done using PHI 5000 Versa Prob II, FEI Inc. ESR spectra was obtained by an A300 electron spin-resonance spectrometer (Bruker, Ettlingen, Germany) at 3450 G and 9.86 GHz. Photocatalytic activity testing was done using Shimadzu-1600 UV–Vis spectrophotometer, Photoluminescence measurements were done using Agilent Cary eclipse Photoluminescent spectrofluorometer equipped with xenon lamp as the source of radiation.

FTIR spectrum of as prepared  $Gd:MgZrO_3$  (1–5 mol% Gd) has been shown in Fig. 1. A broad peak around 335–765  $cm^{-1}$  has been attributed to the presence of vibration modes of metal oxygen bonds (Gd–O, Mg–O and Zr–O). Wide peak around 800–1000  $cm^{-1}$  will be attributed to the hydroxide form of Mg and Zr. The peak at 1100  $cm^{-1}$

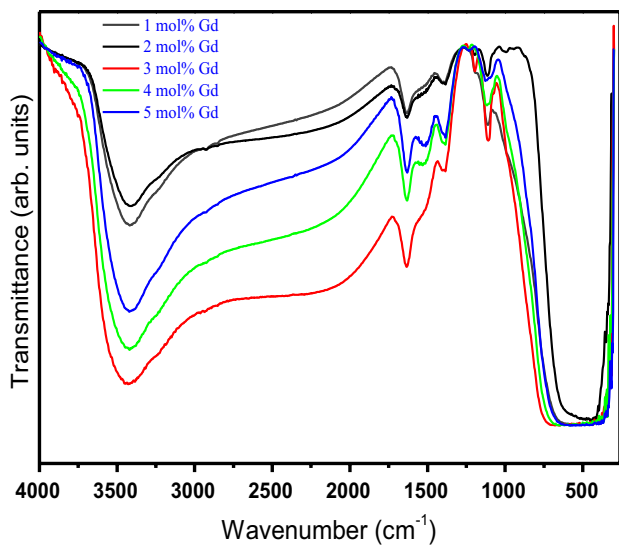


Fig. 1 FTIR spectrum of Gd:MgZrO<sub>3</sub> (1–5 mol%)

is due to the Mg–O–Zr asymmetric stretchings. Peak at 1634 cm<sup>-1</sup> is assigned to the bending mode vibration of water molecules and a significant broad peak at 3420 cm<sup>-1</sup> attributed to the stretching vibrations of –OH involving Mg–OH and Zr–OH. The crystallinity and the phase formation of Gd:MgZrO<sub>3</sub> were studied by X-ray diffraction analysis and is shown in Fig. 2. The patterns clearly indicated dominant cubic zirconia phase with small contribution of cubic magnesium oxide, the structure was in good agreement with the standard JCPDS card No. 27-997 and 1-1235 respectively. No other impurity peaks were visualized in the XRD, this indicates good purity of the prepared material. Upon doping beyond 4% of gadolinium, the XRD peak

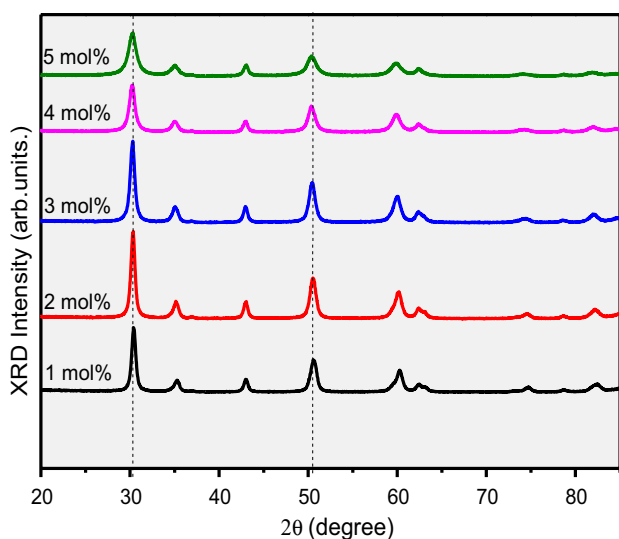


Fig. 2 XRD patterns of Gd:MgZrO<sub>3</sub> (1–5 mol%)

intensity has decreased, this is due to the fact the percolation of dopant ions results in lattice expansion, which consequently induces micro strain and tensile stress in the material. Introducing gadolinium into magnesium zirconate increases its oxygen vacancy defects, these vacancies will reduce the crystal density and expand the lattice. Also, there were no peaks corresponding to gadolinium were observed in the XRD pattern clearly indicates high ordered dispersion of gadolinium in the sea of magnesium zirconate. Scherrer method was used to calculate the average crystallite size of Gd:MgZrO<sub>3</sub>, it was calculated to be 12–16 nm. The microstrain and dislocation density calculated to be  $2.3 \times 10^{-3}$  and 4.7 for Gd:MgZrO<sub>3</sub> (4%).

To investigate the thermal stability of the solvothermal synthesized material, it was subjected to thermo gravimetric analysis (TGA) and is shown in Fig. 3. From the TGA analysis it is evident that, the material lost a percentage weight of 6.1 over ambient temperature to 800 °C. Beyond this temperature the material was almost stable, the gradual loss in weight was attributed to the loss of surface adsorbed water, decomposition of any hydroxide form of material and subsequent phase stabilization of the material, hence the temperature for calcination of the material was opted to be 800 °C.

To obtain information about pore structure, pore volume and specific surface area of Gd:MgZrO<sub>3</sub> (4%), BET surface area and BJH pore size measurements were carried out and the corresponding N<sub>2</sub> adsorption–desorption hysteresis curve has been shown in Fig. 4. From the figure it is clear that, Gd:MgZrO<sub>3</sub> shows type IV adsorption isotherm with H1 type hysteresis, this shows the material is mesoporous in nature with pore distribution centered at 15 nm. The BET surface area calculated to be 162 m<sup>2</sup> g<sup>-1</sup>, to understand the variation surface parameters, BET analysis

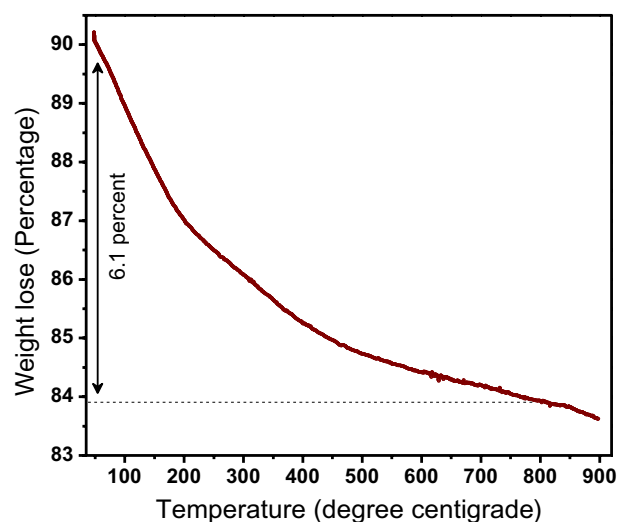
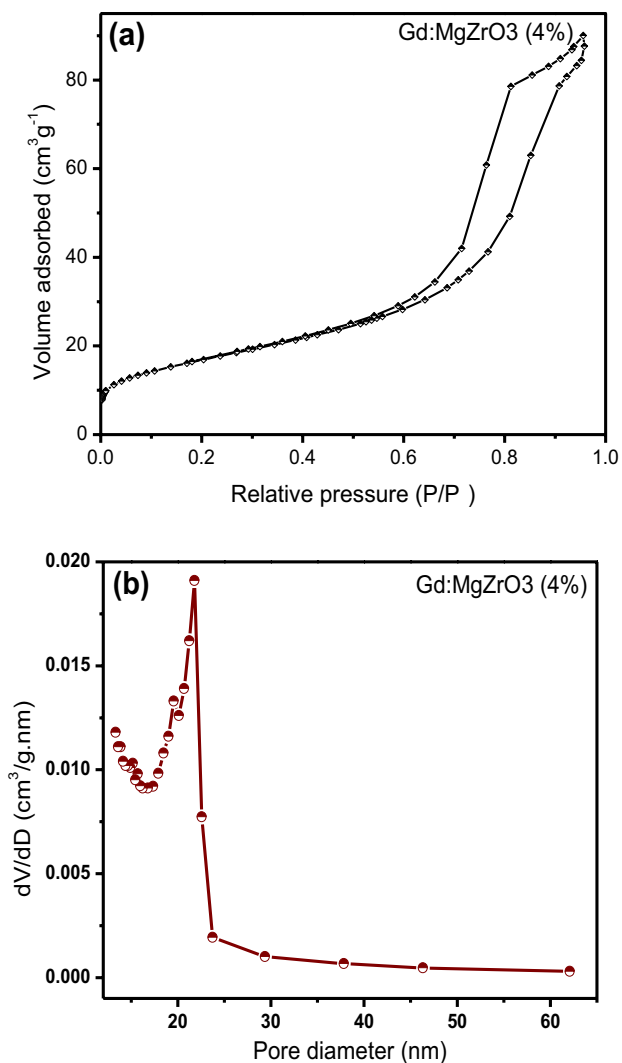


Fig. 3 Thermogravimetric analysis of Gd:MgZrO<sub>3</sub> (4%)



**Fig. 4** **a** N<sub>2</sub> adsorption–desorption isotherm of Gd:MgZrO<sub>3</sub> (4%). **b** BJH pore distribution plot of Gd:MgZrO<sub>3</sub> (4%)

**Table 1** Results of BET analysis of gadolinium doped magnesium zirconate

Sample	Specific surface area (m <sup>2</sup> g <sup>-1</sup> )	Pore volume (cm <sup>3</sup> g <sup>-1</sup> )	Average pore size (nm)
Gd:MgZrO <sub>3</sub> (1%)	156	0.33	9.23
Gd:MgZrO <sub>3</sub> (2%)	152	0.36	10.02
Gd:MgZrO <sub>3</sub> (3%)	142	0.38	10.45
Gd:MgZrO <sub>3</sub> (4%)	162	0.35	9.65
Gd:MgZrO <sub>3</sub> (5%)	160	0.33	9.54

of all the samples has been carried out and presented in Table 1. It is observed from the analysis that, increasing the dopant concentration from 1–3 mol% has decreased the specific surface area owing to strong crystallization of material (as evident from XRD). Further increase to 4 mol%

improved the surface area to 162 m<sup>2</sup> g<sup>-1</sup>, this is attributed to the control of cluster formation at optimum dopant concentration and production of highly specific structures. This high surface area is due to the incorporation of dopants like gadolinium, which restricts the agglomeration and formation of clusters. This high surface area also develops more defect centers, thereby more photoactive sites for effective degradation of dye. Diffuse reflectance spectroscopy (DRS) and Kubelka–Munk function was used to know the band gap of Gd:MgZrO<sub>3</sub> (1–5 mol%) and were shown in Fig. 5a, b. There is slight variation in the band gap of all the five samples but are within 5.45 eV. These variations in the band gap was attributed to the lattice defects, unbalanced charges and order-disorderness created in the material due to the incorporation of gadolinium ions. The

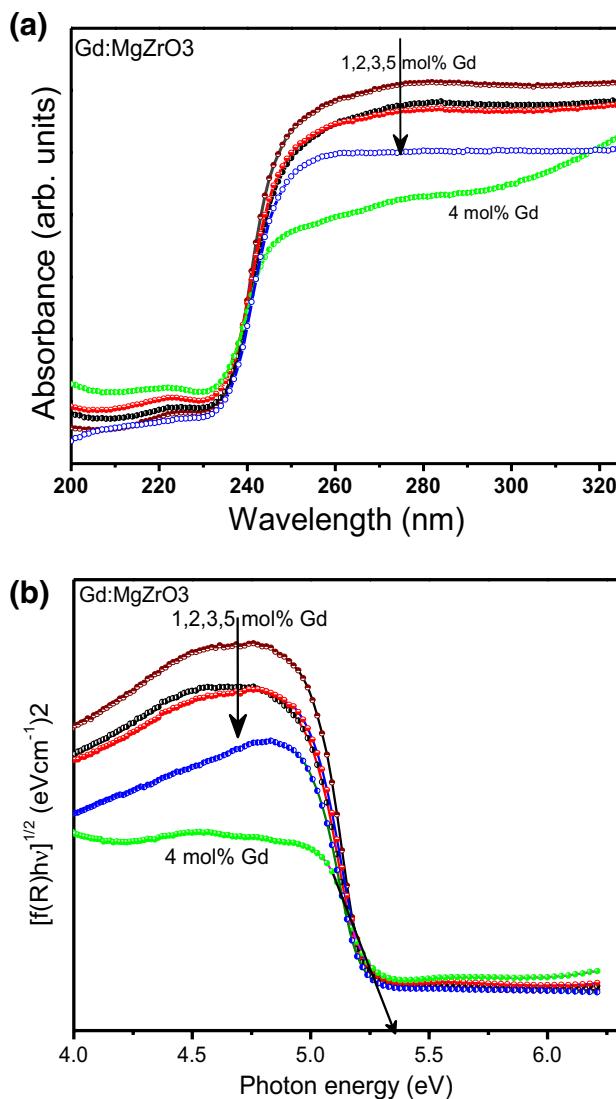


**Fig. 5** **a** Diffuse reflectance spectra of Gd:MgZrO<sub>3</sub> (1–5%). **b** Kubelka–Munk energy band gap plot of Gd:MgZrO<sub>3</sub> (1–5 mol%)



band gap of  $\text{Gd:MgZrO}_3$  (4 mol%) was found to be 5.38 eV. To understand the morphology and microstructure, FESEM images of  $\text{Gd:MgZrO}_3$  (4 mol%) were recorded as shown in Fig. 6. Figure shows the SEM images of  $\text{Gd:MgZrO}_3$

(4 mol%) processed for 12, 24, 48 and 72 h respectively. The material processed for 12 h solvothermal treatment clearly shows particles with nearly rod like irregular agglomerate structures (Fig. 6a), these structures would

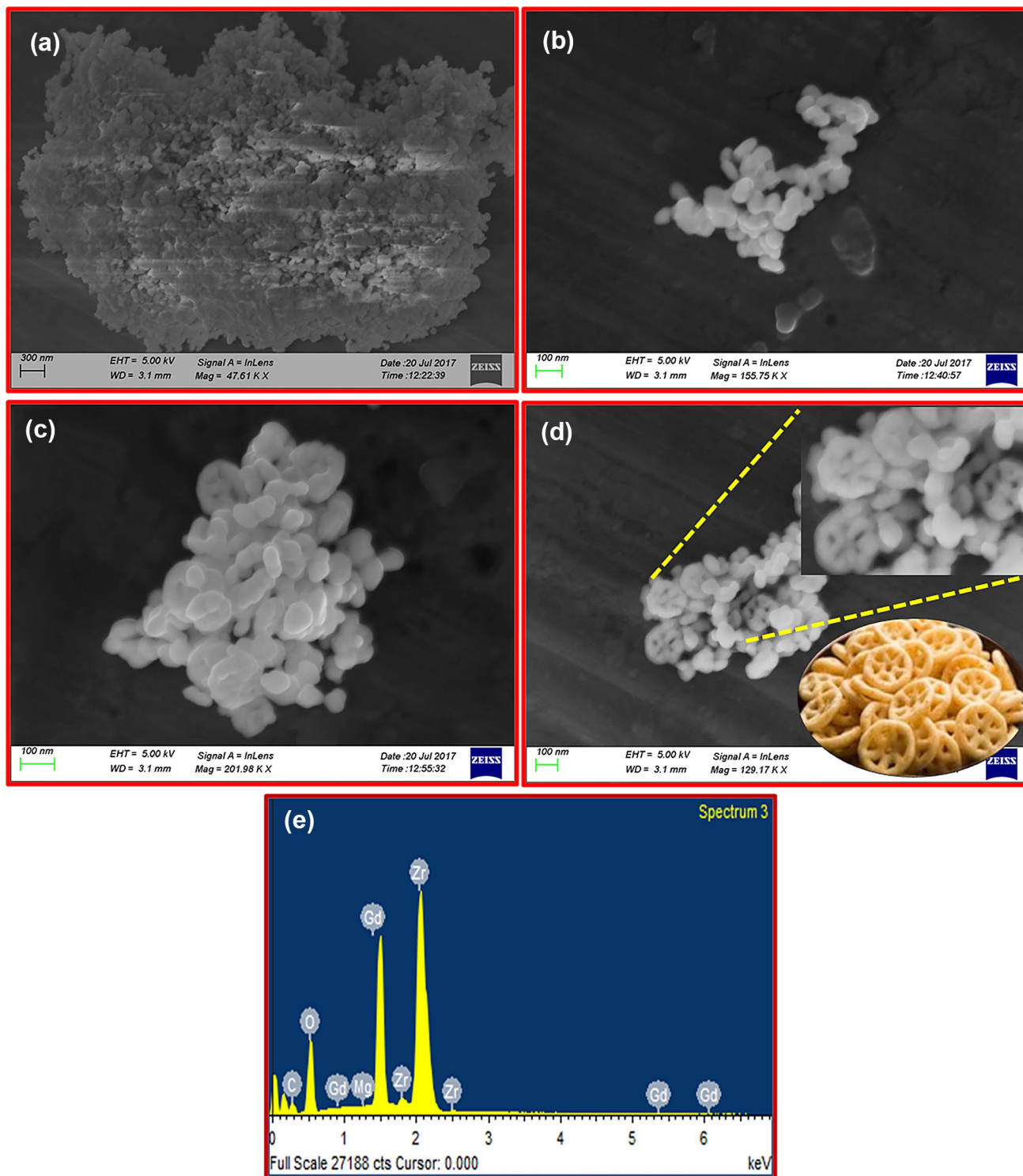


Fig. 6 FESEM images of solvothermal treated  $\text{Gd:MgZrO}_3$  (4%)—a For 12 h, b 24 h, c 48 h, d 72 h

self assemble, cross to form dumble shaped particles when solvothermal processed for 24 h (Fig. 6b). These dumble shaped particle further assemble to give regular circular shaped clusters (Fig. 6c). Owing to the instability of these clusters, they align to give rise to compact disc like structures (Fig. 6d-The inset of the figure shows enlarged image showing disc structures and a representative image also been provided for comparison). From the SEM investigation it is clear that, formation of disc like structure takes place when the precursors were solvothermal treated for a duration of 72 h only. Also it is clearly evident that long duration solvothermal treatment reduced the agglomeration. Figure 6e shows the Energy dispersive spectroscopy (EDX) of Gd:MgZrO<sub>3</sub> (4 mol%), which clearly indicates that, the material is pure and all the elements Gd, O, Mg and Zr were clearly seen in the image. The elemental composition obtained from the EDX was in close correlation with that of experimental calculation. To examine into the deep insights of elemental composition and oxidation state of the elements, XPS analysis of Gd:MgZrO<sub>3</sub> (4 mol%) was carried out. The core level XPS of Gd shown in Fig. 7a clearly indicates two spin orbit doublets at 1220.2 (3d<sub>3/2</sub>) and 1187.5 (3d<sub>5/2</sub>), incorporation and existence of Gd<sup>3+</sup> was clearly evident from this data [26]. The core Mg 1 s XPS spectra shows a typical at 1304.6, indicates monooxide form of magnesium as shown in Fig. 7b [27]. XPS of zirconia shows two spin-orbit split doublets (Fig. 7c) at 182 eV and 184.5 eV corresponding to 3d<sub>5/2</sub> and 3d<sub>3/2</sub> respectively with an energy separation of 2.5 eV. Also the full width at half maximum (FWHM) was found to be 1.7 eV for both peaks, these values were in good agreement with the literature reported [28]. Figure 7d shows the O 1s spectra of Gd:MgZrO<sub>3</sub> (4 mol%) positioned at 530.2 eV, this clearly indicates the formation of oxides of magnesium and zirconium. Also absence of satellite peaks clearly indicates that there are no surface hydroxyl groups or physisorbed water molecules, this is due to fact that the material is calcinated at 800 °C.

Photocatalytic experiments of Gd:MgZrO<sub>3</sub> was performed for the degradation of Rhodamine B a cationic dye under UV light irradiation. Before degradation process the catalyst-dye mixture (20 mg l<sup>-1</sup> of dye) was allowed to attain adsorption-desorption equilibrium for 30 min. The progress of the degradation process was monitored by measuring its UV-vis absorption spectrum. The degradation efficiencies were expressed in terms of percentage of dye degraded, it was found to be 91.6 ± 3.2 for Gd:MgZrO<sub>3</sub> (4 mol%). 4 mol% of gadolinium doped magnesium zirconate was found to be optimum for photocatalytic degradation of Rhodamine B, beyond this percentage of gadolinium doping will decrease the effective available surface area, thereby decreases the photocatalytic efficiency as shown in Fig. 8a. Kinetics of RhB degradation is another

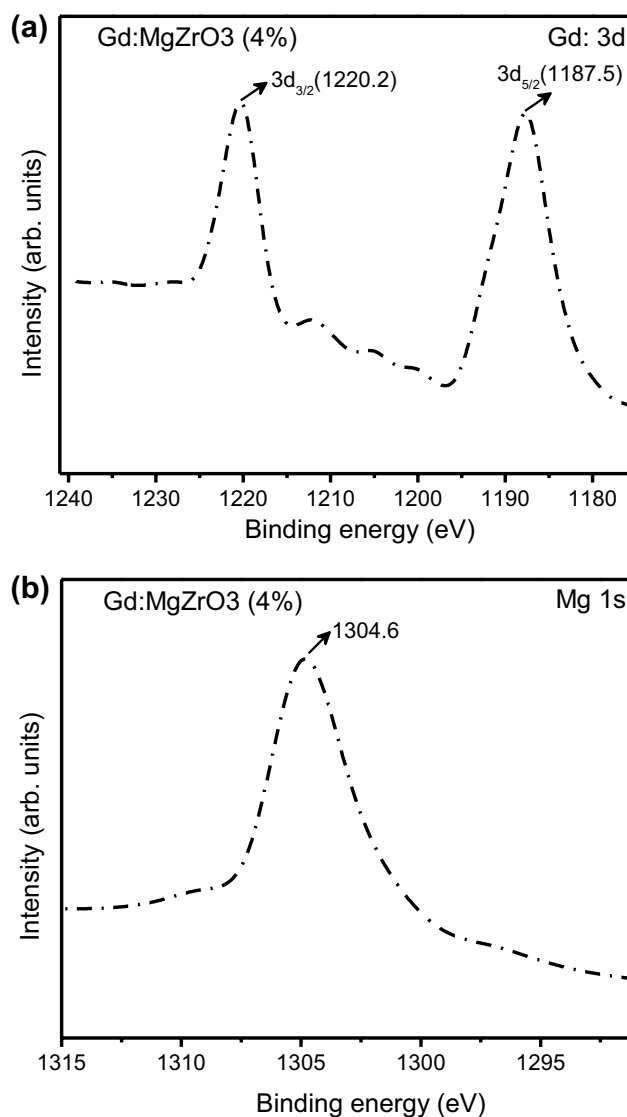
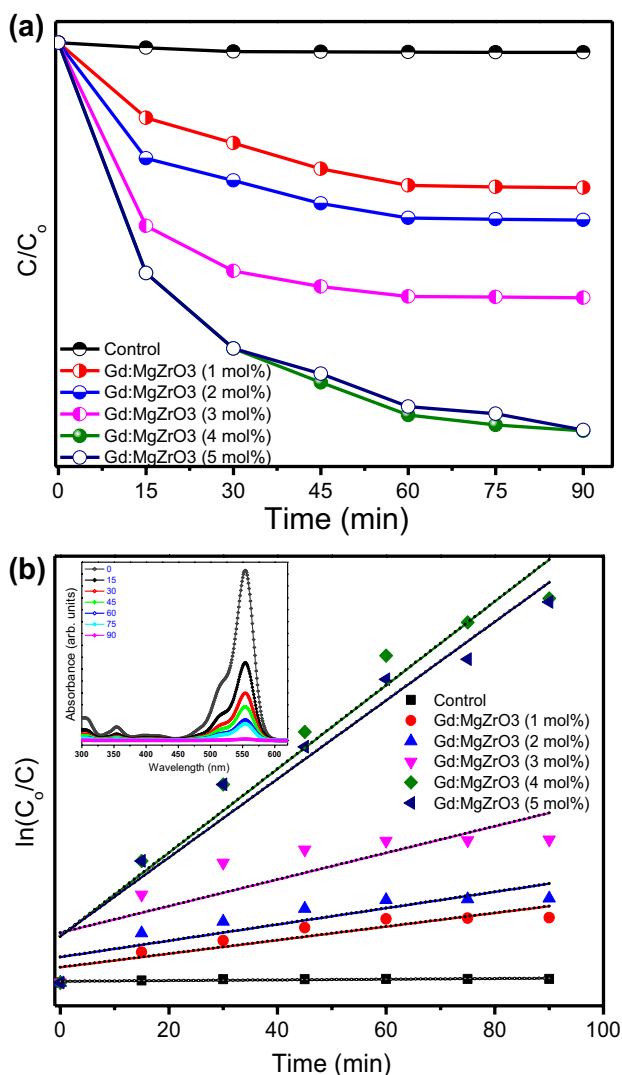
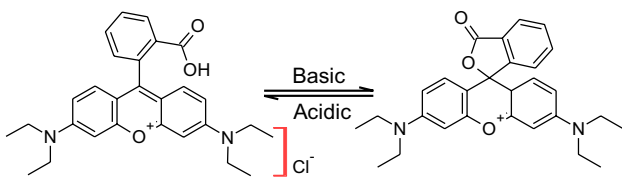


Fig. 7 Core level XPS spectra of **a** Gd-3d, **b** Mg-1s, **c** Zr-3d, **d** O-1s

important parameter which gives deep insights into the underlying mechanism, more than 75% of dye underwent degradation within the initial 45 min (Fig. 8b), this indicates that RhB degradation follows a peculiar mechanism. For now, RhB shows majorly two different structural forms like lactone and zwitterion forms (Fig. 9) based on the pH of the solution [29]. The absorption at 259 nm is arising due to the presence of aromatic rings of Rhodamine B, consequent decrement in the absorption at 259 nm during the degradation process clearly indicates destruction of aromatic rings. The absorption band at 553 nm is due to n → π transition arising due to carboxyl and imine functional groups present in Rhodamine B, decrease in intensity of this peak indicates breakage and subsequent degradation these groups to form CO<sub>2</sub> and H<sub>2</sub>O [30]. From the absorption spectra (inset Fig. 8b) it is clearly evident that,



**Fig. 8** **a** Normalized degradation plots of RhB, **b** Kinetic plots with rate of degradation of RhB (Inset UV-Vis absorption spectra of RhB)



**Fig. 9** Lactone and zwitterion forms of Rhodamine b

there is no shift in the peak position. This clearly indicates direct destruction of aromatic moieties during the degradation of RhB at Gd:MgZrO<sub>3</sub> followed by mineralization. Optimization of reaction with respect to the amount of Gd:MgZrO<sub>3</sub> at constant irradiation of light was made, the optimal amount of catalyst was found to be 50 mg with 91.6% of degradation efficiency with respect to RhB. The

reusability of the catalyst was evaluated, after each batch of photocatalytic experiment, the catalyst was washed with ethanol and dried at 120 °C in an hot air oven. High retention of photocatalytic activity with no significant lose in performance was observed even after five batches of photocatalytic process as shown in Fig. 10.

To know the RhB degradation mechanism at Gd:MgZrO<sub>3</sub>, radical trapping experiments were carried out. Ethylene diamine tetraacetic acid (EDTA), benzoquinone (BQ) and iso-propanol (iP) were used to trap holes, electrons and  $\cdot OH$  radicals respectively. Addition of iso-propanol ( $72.4 \pm 3.2$ ) and benzoquinone ( $76.2 \pm 3.0$ ) didnot influence much on the kinetics of RhB degradation at Gd:MgZrO<sub>3</sub>, however addition of EDTA ( $42.4 \pm 3.4$ ) decreased the reaction significantly (Fig. 11 a). From this observation it is cleary evident that, participation of photogenerated holes are mainly responsible for the degradation of RhB with minor contribution from electrons and  $\cdot OH$  radicals [31]. The retention of crystal structure of the catalyst was confirmed by recording the XRD of the catalyst after five batches of photocatalytic process as shown in Fig. 11b. The generation of hydroxide radicals during the photochemical process was further examined by the ESR technique, (5,5-Dimethyl-1-pyrroline N-oxide) DMPO was used as a probe reagent in spin-trap experiments in aqueous solution. As shown in Fig. 12 no DMPO- $\cdot OH$  adducts were detected for the degradation experiment conducted in dark condition in presence of Gd:MgZrO<sub>3</sub>. However, under UV irradiation, the characteristic quartet peaks of DMPO- $\cdot OH$  with intensity distribution of (1:2:2:1) are observed. From the ESR characterization it is clearly evident that, involent oxygeneous radical ( $\cdot OH$ ) during

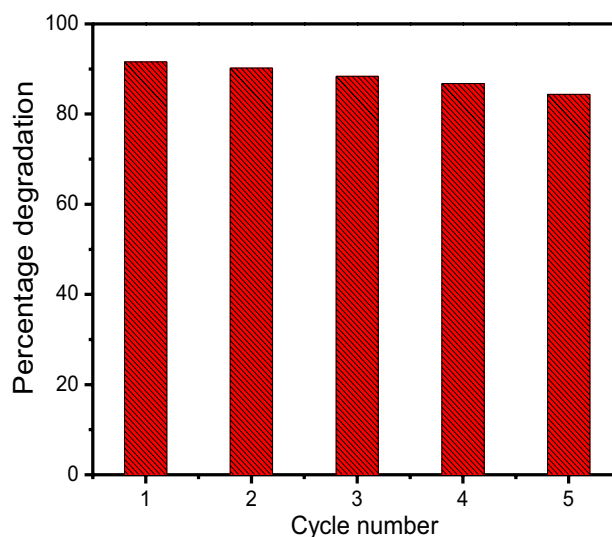


**Fig. 10** Reusability test of degradation of RhB at Gd:MgZrO<sub>3</sub>

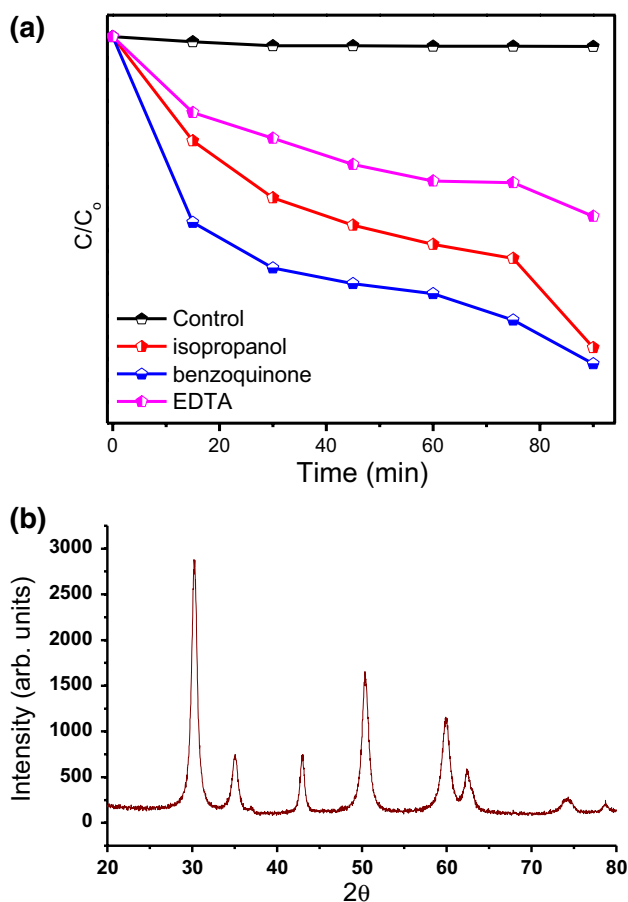


**Fig. 11** **a** Normalized photocatalytic degradation of RhB in presence of scavengers (IP, BQ and EDTA) at Gd:MgZrO<sub>3</sub>. **b** XRD spectrum of Gd:MgZrO<sub>3</sub> after five cycles of photocatalytic process

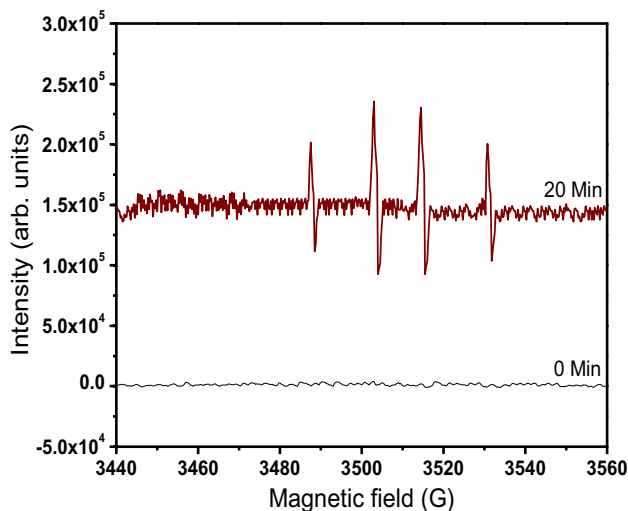


**Fig. 12** ESR spectra of hydroxyl radicals-adduct with DMPO at Gd:MgZrO<sub>3</sub> (4 mol%) in aqueous dispersion under the irradiation of UV light (254 nm, 500 mW/cm<sup>2</sup>). Volume-2 mL, Gd:MgZrO<sub>3</sub>-4 mg, DMPO-0.22 M

the photocatalytic degradation of Rhodamine B in water at Gd:MgZrO<sub>3</sub>.

To know the nature of charge transfer and rate of recombination of electron-hole pairs, photoluminescence spectra of Gd:MgZrO<sub>3</sub> has been recorded. The PL spectra of Gd:MgZrO<sub>3</sub> excited at λ<sub>excitation</sub> = 270 nm has been shown in Fig. 13. The photons with this energy can bring about the transition between the valence and conduction states. From the spectra it is clearly evident that, combination of Gd (Valence + 3), Mg (Valence + 2) with Zr (Valence + 4) will create more oxygen vacancy defects to excite more F-centers, this would result in improved luminescence intensity (Inset of Fig. 13). The energy peaks positioned at 2.93 eV and 2.79 eV are due to the singly ionized vacancy centers (Vo<sup>+</sup>) and arise due to multiple luminescence centers. The band at 3.36 eV is due to the cumulative effect of uneven distribution of Zr<sup>4+</sup> at near surface sites, which arise due to the dangling bonds on the surface of the material and due to the radiative recombination of electrons and holes in gadolinium centers. The green emission at 2.24 eV is due to <sup>6</sup>G<sub>7</sub> to Gd<sup>3+</sup> transition that arise due to stark level manifolds [32–36]. From PL studies it is found that combination of Gd, Mg and Zr resulted in high oxygen vacancy in the material, this made the Gd:MgZrO<sub>3</sub> a robust photocatalyst for the degradation of RhB.

Degradation of Rhodamine B is achieved by the interaction of RhB with the photogenerated holes of Gd:MgZrO<sub>3</sub>, the recombination of these photogenerated electron-holes will be restrained due to the creation of 4f trap centers created by Gd<sup>3+</sup> ions (Fig. 14), this mechanism leads to the p-n junction like set up. In total the electron-hole recombination is effectively suppressed by the synergism arising by the combination of Gd, Mg

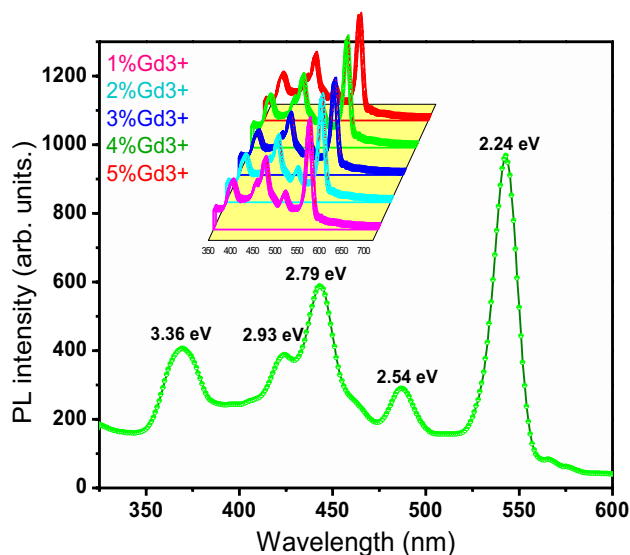


**Fig. 13** Photoluminescence spectra of Gd:MgZrO<sub>3</sub> (1–5 mol%)



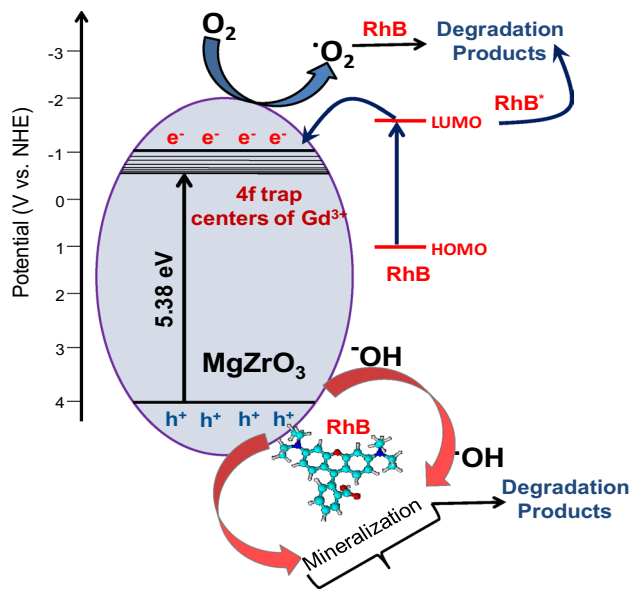


**Fig. 14** Proposed mechanism of degradation of RhB at Gd:MgZrO<sub>3</sub>

and Zr. From the experimental investigation it is evident that, the photogenerated holes and electrons are arising either from the Gd:MgZrO<sub>3</sub> material or Rhodamine B dye. Finally it is clearly proved that, the degradation of RhB is majorly governed by (i) interaction of RhB with the photogenerated holes in Gd:MgZrO<sub>3</sub> and with minor contribution from (ii) Ionization of O<sub>2</sub> and its interaction with RhB (iii) Transfer of electrons from LUMO levels of photoexcited RhB to the conduction band or defect levels of Gd:MgZrO<sub>3</sub> followed by mineralization.

### 3 Conclusions

Nanoscale disc like gadolinium doped magnesium zirconate was prepared by simple solvothermal process. Optimization of reaction conditions revealed that, 4 mol% Gd:MgZrO<sub>3</sub> was effective for the photocatalytic degradation of Rhodamine B than other combinations. The robust photocatalytic efficiency is due to the synergistic effect arising due to high defect centers created by the combination of these elements. When the precursors are processed by solvothermal protocol for three days lead to the formation of disc like Gd:MgZrO<sub>3</sub>, which lead to high degradation efficiency against the cationic dye RhB (91.6%), good reusability and stability. All these properties makes Gd:MgZrO<sub>3</sub> a competent material in environmental remediation.

### Compliance with ethical standards

**Conflict of interest** The authors declare that they have no conflicts of interest.

### References

- Lellis B, Fávaro-Polonio CZ, Pamphile JA, Polonio JC (2019) Effects of textile dyes on health and the environment and bioremediation potential of living organisms. *Biotechnol Res Innov* 3:275–290. <https://doi.org/10.1016/j.biori.2019.09.001>
- Ahmad A, Mohd-Setapar SH, Chuong CS, Khatoun A, Wani WA, Kumar R, Rafatullah M (2015) Recent advances in new generation dye removal technologies: novel search for approaches to reprocess wastewater. *RSC Adv* 5:30801–30818. <https://doi.org/10.1039/c4ra16959j>
- Saleem J, Bin Shahid U, Hijab M, Mackey H, McKay G (2019) Production and applications of activated carbons as adsorbents from olive stones. *Biomass Convers Biorefinery* 9:775–802. <https://doi.org/10.1007/s13399-019-00473-7>
- Saritha V, Karnena MK, Dwarapureddi BK (2020) Competence of blended coagulants for surface water treatment. *Appl Water Sci* 10:20. <https://doi.org/10.1007/s13201-019-1108-4>
- Srivastava S, Vaddadi S, Kumar P, Sadistap S (2018) Design and development of reverse osmosis (RO) plant status monitoring system for early fault prediction and predictive maintenance. *Appl Water Sci* 8:1–10. <https://doi.org/10.1007/s13201-018-0821-8>
- Loeb SK, Alvarez PJJ, Brame JA, Cates EL, Choi W, Crittenden J, Dionysiou DD, Li Q, Li-Puma G, Quan X, Sedlak DL, David Waite T, Westerhoff P, Kim JH (2019) The technology horizon for photocatalytic water treatment: sunrise or sunset? *Environ Sci Technol* 53:2937–2947. <https://doi.org/10.1021/acs.est.8b05041>
- Zaleska-Medynska A, Marchelek M, Diak M, Grabowska E (2016) Noble metal-based bimetallic nanoparticles: the effect of the structure on the optical, catalytic and photocatalytic properties. *Adv Colloid Interface Sci* 229:80–107. <https://doi.org/10.1016/j.cis.2015.12.008>
- Wali LA, Alwan AM, Dheyab AB, Hashim DA (2019) Excellent fabrication of Pd-Ag NPs/PSi photocatalyst based on bimetallic nanoparticles for improving methylene blue photocatalytic degradation. *Optik* 179:708–717. <https://doi.org/10.1016/j.ijleo.2018.11.011>
- Sharma G, Gupta VK, Agarwal S, Bhogal S, Naushad M, Kumar A, Stadler FJ (2018) Fabrication and characterization of trimetallic nano-photocatalyst for remediation of ampicillin antibiotic. *J Mol Liq* 260:342–350. <https://doi.org/10.1016/j.molliq.2018.03.059>
- Kumar D, Awasthi GP, Park CH, Kim CS (2018) Multifunctional trimetallic colloidal plasmonic nano-hybrid: highly efficient photocatalyst and photothermal agent. *Adv Mater Interfaces* 5:1–7. <https://doi.org/10.1002/admi.201800331>
- Kumar KY, Saini H, Pandiarajan D, Prashanth MK, Parashuram L, Raghu MS (2018) Controllable synthesis of TiO<sub>2</sub> chemically bonded graphene for photocatalytic hydrogen evolution and dye degradation. *Catal Today*. <https://doi.org/10.1016/j.cattod.2018.10.042>
- Yoo JE, Lee K, Altomare M, Selli E, Schmuki P (2013) Self-organized arrays of single-metal catalyst particles in TiO<sub>2</sub> cavities: a highly efficient photocatalytic system. *Angew Chemie Int Ed* 52:7514–7517. <https://doi.org/10.1002/anie.201302525>
- Rao T, Saladino ML, Wang X, Fang Y, Giordano C (2019) Multimetallic oxynitrides nanoparticles for a new generation

- of photocatalysts. *Chemistry* 25:16676–16682. <https://doi.org/10.1002/chem.201904033>
14. Jiang L, Li J, Wang K, Zhang G, Li Y, Wu X (2020) Environmental low boiling point solvent mediated strategy to synthesize functionalized monolayer carbon nitride for superior photocatalytic hydrogen evolution. *Appl Catal B* 260:118181. <https://doi.org/10.1016/j.apcatb.2019.118181>
  15. Jiang T, Wang K, Guo T, Wu X, Zhang G (2020) Fabrication of Z-scheme  $\text{MoO}_3/\text{Bi}_2\text{O}_4$  heterojunction photocatalyst with enhanced photocatalytic performance under visible light irradiation. *Chin J Catal* 41:161–169. [https://doi.org/10.1016/S1872-2067\(19\)63391-7](https://doi.org/10.1016/S1872-2067(19)63391-7)
  16. Parashuram L, Sreenivasa S, Akshatha S, Kumar VU, Kumar S (2017) Zirconia-supported Cu(I)-stabilized copper oxide mesoporous catalyst for the synthesis of quinazolinones under ambient conditions. *Asian J Org Chem* 6:1755–1759. <https://doi.org/10.1002/ajoc.201700467>
  17. Parashuram L, Sreenivasa S, Akshatha S, Udayakumar V, Sandeep Kumar A (2019) A non-enzymatic electrochemical sensor based on  $\text{ZrO}_2$ : Cu(I) nanosphere modified carbon paste electrode for electro-catalytic oxidative detection of glucose in raw Citrus aurantium var. sinensis. *Food Chem* 300:125178. <https://doi.org/10.1016/j.foodchem.2019.125178>
  18. Dhandapani C, Narayanasamy R, Karthick SN, Hemalatha KV, Selvam S, Hemalatha P, Suresh M, Kirupha SD, Kim H (2016) Drastic photocatalytic degradation of methylene blue dye by neodymium doped zirconium oxide as photocatalyst under visible light irradiation. *Opt Int J Light Electron Opt* 127:10288–10296. <https://doi.org/10.1016/j.ijleo.2016.08.048>
  19. Parashuram L, Sreenivasa S, Akshatha SR, Kumar VU, Kumar S (2019) Environmentally benign approach for the synthesis of Azo dyes in the presence of mesoporous sulfated core-shell zirconia-copper(I) oxide solid acid catalyst. *ChemistrySelect* 4:5097–5105. <https://doi.org/10.1002/slct.201803295>
  20. Shim JH, Chao CC, Huango H, Prinz FB (2007) Atomic layer deposition of yttria-stabilized zirconia for solid oxide fuel cells. *Chem Mater* 19:3850–3854. <https://doi.org/10.1021/cm070913t>
  21. Huang Z, Han W, Feng Z, Qi J, Wu D, Wei N, Tang Z, Zhang Y, Duan J, Lu T (2019) The effects of precipitants on co-precipitation synthesis of yttria-stabilized zirconia nanocrystalline powders. *J Sol-Gel Sci Technol* 90:359–368. <https://doi.org/10.1007/s10971-019-04947-y>
  22. Chang Y, Wang C, Liang T, Zhao C, Luo X, Guo T, Gong J, Wu H (2015) Sol-gel synthesis of mesoporous spherical zirconia. *RSC Adv* 5:104629–104634. <https://doi.org/10.1039/c5ra23782c>
  23. Akshatha S, Sreenivasa S, Parashuram L, Udaya Kumar V, Sharma SC, Nagabhushana H, Kumar S, Maiyalagan T (2019) Synergistic effect of hybrid  $\text{Ce}^{3+}/\text{Ce}^{4+}$  doped  $\text{Bi}_2\text{O}_3$  nano-sphere photocatalyst for enhanced photocatalytic degradation of alizarin red S dye and its NUV excited photoluminescence studies. *J Environ Chem Eng* 7:103053. <https://doi.org/10.1016/j.jece.2019.103053>
  24. Sagadevan S, Podder J, Das I (2016) Hydrothermal synthesis of zirconium oxide nanoparticles and its characterization. *J Mater Sci Mater Electron* 27:5622–5627. <https://doi.org/10.1007/s10854-016-4469-6>
  25. Liu X, Pappas I, Fitzgerald M, Zhu Y, Eibling M, Pan L (2010) Solvothermal synthesis and characterization of  $\text{ZrO}_2$  nanostructures using zirconium precursor. *Mater Lett* 64:1591–1594. <https://doi.org/10.1016/j.matlet.2010.04.044>
  26. Barreca D, Gasparotto A, Milanov A, Tondello E, Devi A, Fischer RA (2007)  $\text{Gd}_2\text{O}_3$  nanostructured thin films analyzed by XPS. *Surf Sci Spectra* 14:60–67. <https://doi.org/10.1116/11.20080703>
  27. Ardizzone S, Bianchi CL, Fadoni M, Vercelli B (1997) Magnesium salts and oxide: an XPS overview. *Appl Surf Sci* 119:253–259. [https://doi.org/10.1016/S0169-4332\(97\)00180-3](https://doi.org/10.1016/S0169-4332(97)00180-3)
  28. Sinhamahapatra A, Jeon J, Kang J, Han B, Yu J (2016) Oxygen-deficient zirconia ( $\text{ZrO}_2-x$ ): a new material for solar light absorption. *Sci Rep* 6:1–8. <https://doi.org/10.1038/srep27218>
  29. Hinckley DA, Seybold PG (1988) A spectroscopic/thermodynamic study of the rhodamine B lactone e zwitterion equilibrium. *Spectrochim Acta Part A* 44:1053–1059
  30. Chen X, Xue Z, Yao Y, Wang W, Zhu F, Hong C (2012) Oxidation degradation of rhodamine B in aqueous by UV/S $2\text{O}_8^{2-}$  treatment system. *Int J Photoenergy* 2012:1–5. <https://doi.org/10.1155/2012/754691>
  31. Sharma M, Vaidya S, Ganguli AK (2017) Enhanced photocatalytic activity of g-C $3\text{N}_4$ -TiO $2$  nanocomposites for degradation of Rhodamine B dye. *J Photochem Photobiol A* 335:287–293. <https://doi.org/10.1016/j.jphotochem.2016.12.002>
  32. Tamrakar RK, Bisen DP, Brahme N (2014) Comparison of photoluminescence properties of  $\text{Gd}_2\text{O}_3$  phosphor synthesized by combustion and solid state reaction method. *J Radiat Res Appl Sci* 7:550–559. <https://doi.org/10.1016/j.jrras.2014.09.005>
  33. Manjunatha S, Dharmaparakash MS (2012) Thermal stability, optical and photoluminescence properties of spherical  $\text{Ce}_x\text{Zr}_{1-x}\text{O}_2$  ( $x=0.05$ ) crystalline blue-emitting nanophosphors synthesized by microwave method. *Mater Res Express* 2:1–46
  34. Liang J, Deng Z, Jiang X, Li F, Li Y (2002) Photoluminescence of tetragonal  $\text{ZrO}_2$  nanoparticles synthesized by microwave irradiation. *Inorg Chem* 41:3602–3604. <https://doi.org/10.1021/ic025532q>
  35. Zhang H, Fu X, Niu S, Xin Q (2008) Blue emission of  $\text{ZrO}_2$ : Tm nanocrystals with different crystal structure under UV excitation. *J Non Cryst Solids* 354:1559–1563. <https://doi.org/10.1016/j.jnoncrysol.2007.08.064>
  36. Emeline A, Kataeva GV, Litke AS, Ryabchuk VK, Rudakova AV, Serpone N (1998) Spectroscopic and photoluminescence studies of a wide band gap insulating material: powdered and colloidal  $\text{ZrO}_2$  sols. *Langmuir* 14:5011–5022. <https://doi.org/10.1021/la980083i>

**Publisher's Note** Springer Nature remains neutral with regard to jurisdictional claims in published maps and institutional affiliations.